Supporting Information for

Combined Temperature and Pressure Sensing Using Luminescent $NaBiF_4$:Yb,Er Nanoparticles

Magda A. Antoniak[1,*], *Szymon J. Zelewski*[2,*], *Robert Oliva*[2], *Andrzej Żak*[3], *Robert Kudrawiec*[2], *Marcin Nyk*[1,**]

[1]Advanced Materials Engineering and Modelling Group, Faculty of Chemistry, Wrocław University of Science and Technology, Wybrzeże Wyspiańskiego 27, 50-370 Wrocław, Poland

[2]Department of Semiconductor Materials Engineering, Faculty of Fundamental Problems of Technology, Wrocław University of Science and Technology, Wybrzeże Wyspiańskiego 27, 50-370 Wrocław, Poland

[3] Electron Microscopy Laboratory, Faculty of Mechanical Engineering, Wrocław University of Science and Technology, Wybrzeże Wyspiańskiego 27, 50-370 Wrocław, Poland

*These authors contributed equally to this work.

**Corresponding author.

E-mail address: marcin.nyk@pwr.edu.pl

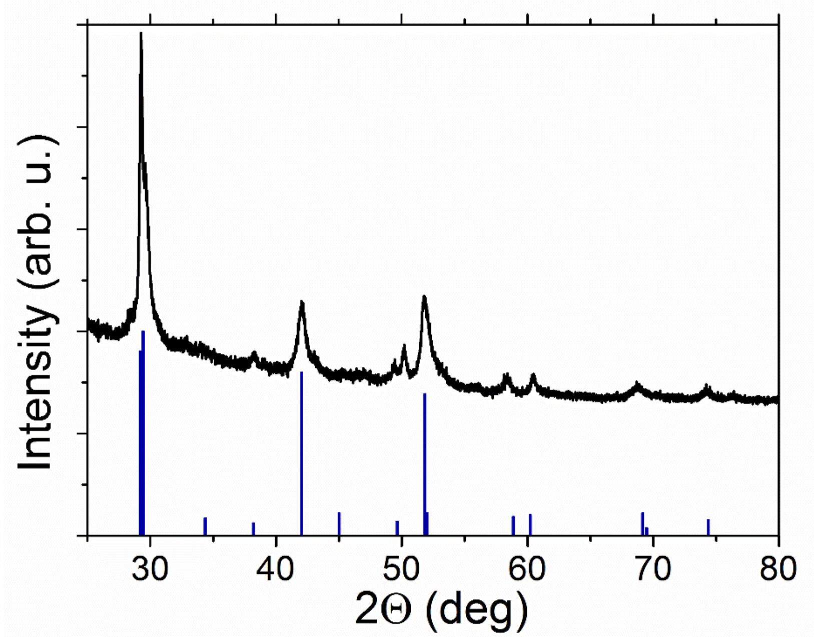

Figure S1. Experimental powder X-ray diffraction pattern of $NaBiF_4$:Yb,Er NPs in comparison with the crystalline reference pattern of hexagonal (β) phase $NaBiF_4$ (JCPDS no. 41-0796). The XRD peak at 50.16° comes from a silicon sample holder.

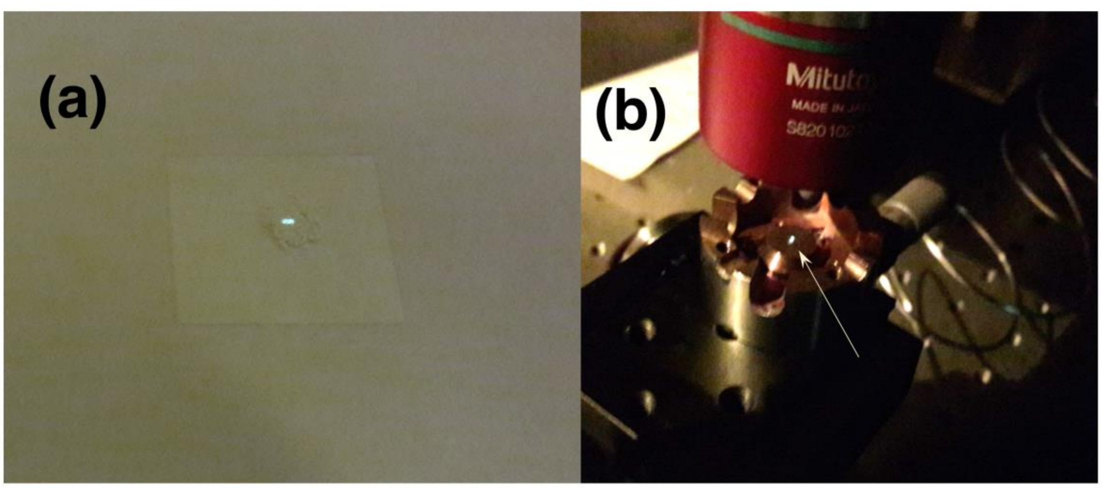

Figure S2. Emission images of $NaBiF_4$:Yb,Er NPs under 980 nm, 5 W/cm^2 excitation power density (a) and under experimental conditions used in high pressure measurements (b).

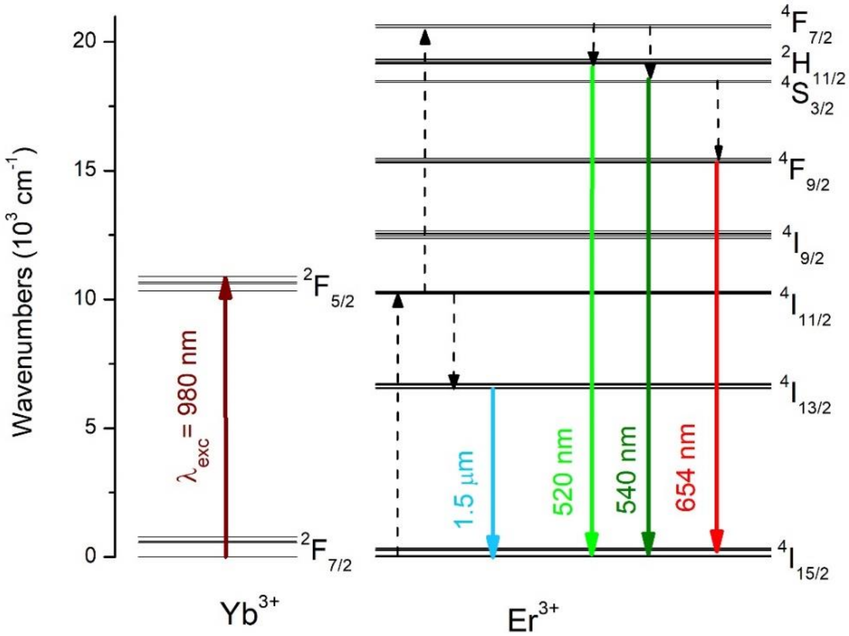

Figure S3. Yb-Er energy level diagram and proposed energy transfer mechanisms under 980 nm CW laser diode excitation.

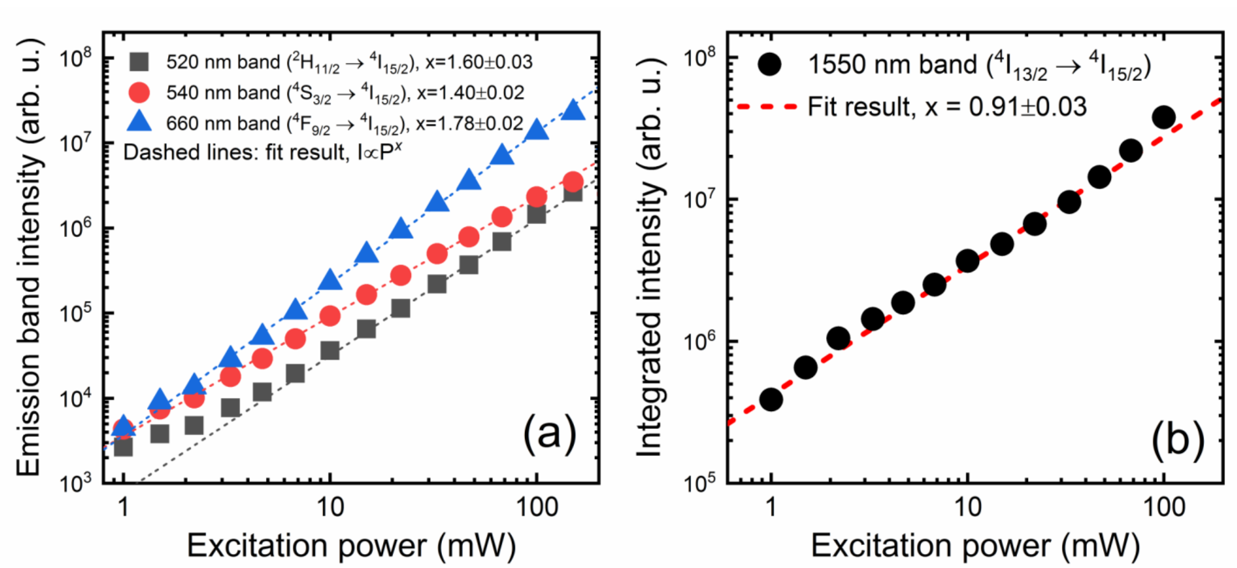

Figure S4. Log-log plots of integrated emission intensity of visible range (a) and infrared (b) electronic transitions as a function of 980 nm CW laser excitation power. (1-R^2) values: 6.6×10^{-4}, 520 nm band; 2.4×10^{-4}, 540 nm band; 1.8×10^{-4}, 660 nm band; 3.8×10^{-3}, 1550 nm band.

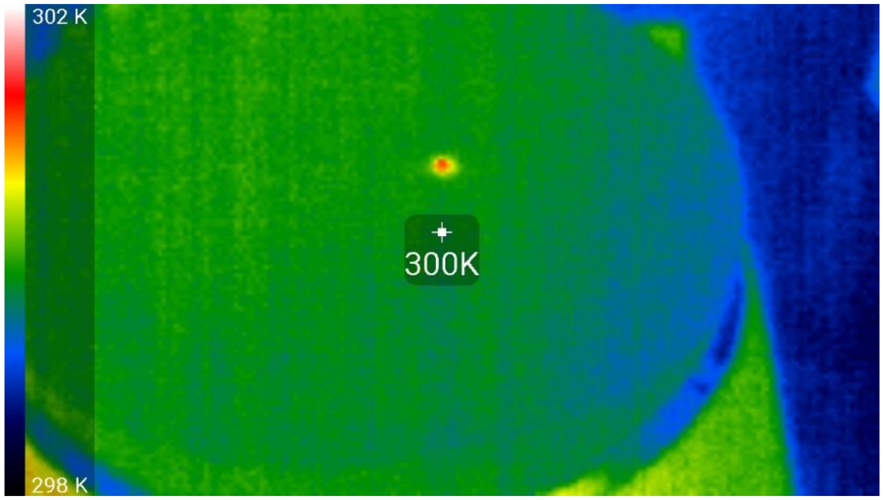

Figure S5. Room temperature infrared thermal image (taken with a Seek Thermal Compact microbolometer camera) showing laser-induced sample heating under conditions set for temperature-dependent experiments with 100 mW laser beam.

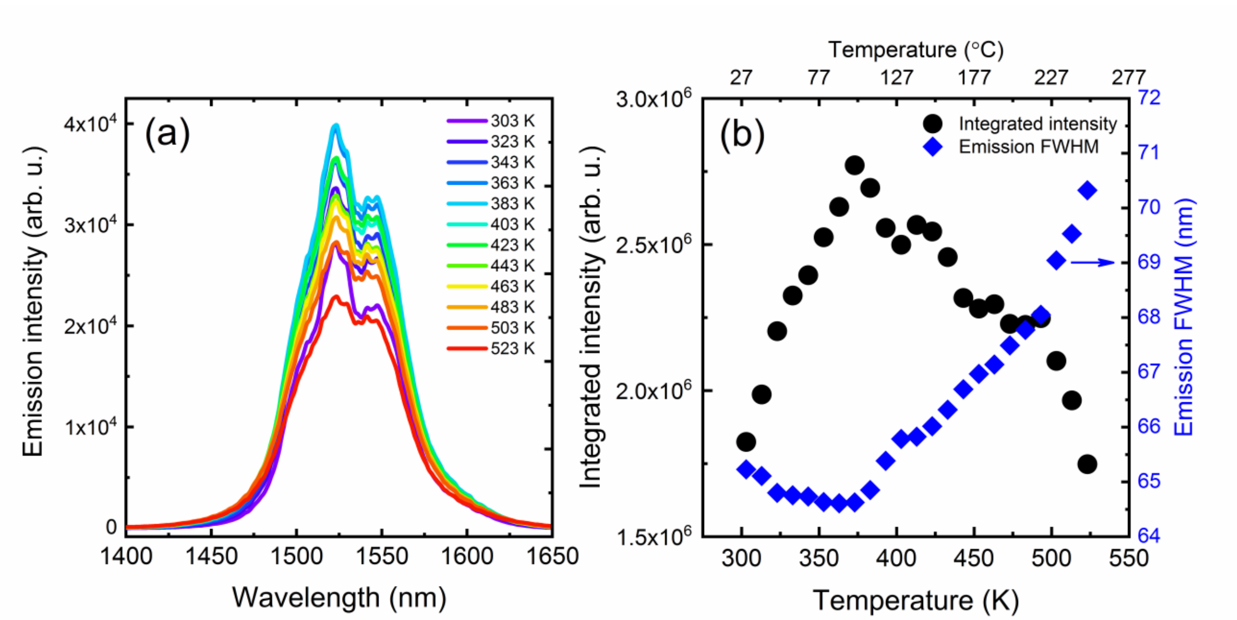

Figure S6. Temperature-dependent infrared emission from the Er^{3+} $^4I_{13/2}\rightarrow{}^4I_{15/2}$ transition (a) along with determined integrated band emission intensity and broadening (b).

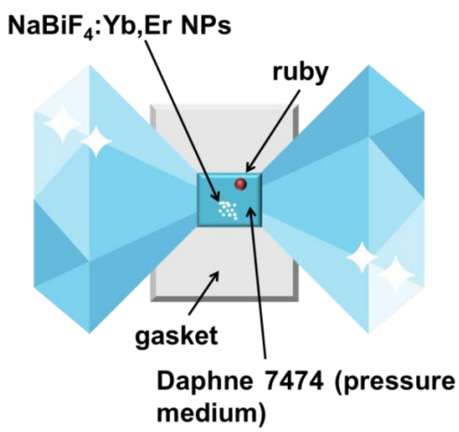

Figure S7. Schematic diagram for high-pressure luminescence measurements of $NaBiF_4$:Yb,Er NPs in the diamond anvil cell.

Table S1. The relative sensitivity and reliable operation temperature range of optical temperature sensors based on LIR (I_{520}/I_{540}) ytterbium (III) and erbium (III) doped nano/microcrystals.

Optical temperature sensor	**Temperature range (K)**	**Maximal value of relative sensitivity S_R (K^{-1})**	**Ref.**
$NaY(WO_4)_2$:Yb,Er	293 -503	1.2% at 293 K	[1]
$NaYF_4$:Yb,Er	293 - 753	1.3% at 293 K	[2]
$NaYF_4$:Yb,Er	303 - 328	1.35% at 303 K	[3]
CaF_2:Yb,Er	295 - 723	1.4% at 300 K	[4]
$NaGdF_4:Yb^{3+}:Er^{3+}$@ SiO_2–$Eu(tta)_3$	293-323	1.48% at 303 K	[5]
$NaBiF_4$:Yb,Er	303 - 483	1.24% at 303 K	[6]
$NaBiF_4$:Yb,Er	303 - 523	1.07% at 303 K	This work

Table S2. Fitted formulas for pressure-induced sublevel shift of Er^{3+} emission bands.

Emission band	Peak designation	Fitted formula (x: Pressure in GPa)	Fit quality ($1-R^2$)
$^2H_{11/2}\rightarrow{}^4I_{15/2}$	A	516.955 (−0.0383 nm/GPa)x	0.013
	B	520.002 (+0.0316 nm/GPa)x (−0.00157 nm/GPa^2)x^2	0.042
	C	522.559 (+0.0925 nm/GPa)x	0.012
$^4S_{3/2}\rightarrow{}^4I_{15/2}$	D	539.231 (−0.0199 nm/GPa)x (−0.000969 nm/GPa^2)x^2	0.021
	E	541.865 (+0.0277 nm/GPa)x	0.017
	F	544.449 (+0.107 nm/GPa)x	0.013
	G	549.086 (+0.167 nm/GPa)x	0.016
	H	555.520 (+0.106 nm/GPa)x	0.022
$^4F_{9/2}\rightarrow{}^4I_{15/2}$	I	653.474 (−0.0367 nm/GPa)x (+0.00335 nm/GPa^2)x^2	0.156
	J	660.593 (+0.226 nm/GPa)x	0.014
$^4I_{13/2}\rightarrow{}^4I_{15/2}$	K	1503.28 (−0.780 nm/GPa)x	0.016
	L	1521.71 (−0.398 nm/GPa)x	0.018
	M	1542.99 (+0.934 nm/GPa)x (-0.0378 nm/GPa^2)x^2	0.055

Table S3. Fitted formulas for pressure-induced emission bands broadening.

Emission band	Fitted formula (x: Pressure in GPa)	Fit quality ($1-R^2$)
$^2H_{11/2}\rightarrow{}^4I_{15/2}$	10.109 (+0.139 nm/GPa)x	0.425
$^4S_{3/2}\rightarrow{}^4I_{15/2}$	6.893 (+0.068 nm/GPa)x	0.124
$^4F_{9/2}\rightarrow{}^4I_{15/2}$	14.663 (+0.330 nm/GPa)x	0.077
$^4I_{13/2}\rightarrow{}^4I_{15/2}$	63.122 (+1.359 nm/GPa)x	0.018

References

(1) Lin, M.; Xie, L.; Wang, Z.; Richards, B. S.; Gao, G.; Zhong, J. Facile synthesis of mono-disperse sub-20 nm $NaY(WO_4)_2:Er^{3+},Yb^{3+}$ upconversion nanoparticles: a new choice for nanothermometry. J. Mater. Chem. C 2019, 7 (10), 2971-2977, DOI: 10.1039/C8TC05669B.

(2) Fan, S.; Gao, G.; Sun, S.; Fan, S.; Sun, H.; Hu, L. Absolute up-conversion quantum efficiency reaching 4% in β-$NaYF_4:Yb^{3+},Er^{3+}$ micro-cylinders achieved by Li^+/Na^+ ion-exchange. J. Mater. Chem. C 2018, 6 (20), 5453-5461, DOI: 10.1039/C8TC01806E.

(3) Klier, D. T.; Kumke, M. U. Upconversion Luminescence Properties of $NaYF_4$:Yb:Er Nanoparticles Codoped with Gd^{3+}. The Journal of Physical Chemistry C 2015, 119 (6), 3363-3373, DOI: 10.1021/jp5103548.

(4) Cai, J.; Wei, X.; Hu, F.; Cao, Z.; Zhao, L.; Chen, Y.; Duan, C.; Yin, M. Up-conversion luminescence and optical thermometry properties of transparent glass ceramics containing

$CaF_2:Yb^{3+}/Er^{3+}$ nanocrystals. Ceramics International 2016, 42 (12), 13990-13995, DOI: https://doi.org/10.1016/j.ceramint.2016.06.002.

(5) Nigoghossian, K.; Messaddeq, Y.; Boudreau, D.; Ribeiro, S. J. L. UV and Temperature-Sensing Based on $NaGdF_4:Yb^{3+}:Er^{3+}@SiO_2–Eu(tta)_3$. ACS Omega 2017, 2 (5), 2065-2071, DOI: 10.1021/acsomega.7b00056.

(6) Lei, P.; An, R.; Zhai, X.; Yao, S.; Dong, L.; Xu, X.; Du, K.; Zhang, M.; Feng, J.; Zhang, H. Benefits of surfactant effects on quantum efficiency enhancement and temperature sensing behavior of $NaBiF_4$ upconversion nanoparticles. J. Mater. Chem. C 2017, 5 (37), 9659-9665, DOI: 10.1039/C7TC03122J.